Dielectric losses in multi-layer Josephson junction qubits

David Gunnarsson[1]**, Juha-Matti Pirkkalainen**[2]**, Jian Li**[2]**,
Gheorghe Sorin Paraoanu**[2]**, Pertti Hakonen**[2]**, Mika Sillanpää**[3] **and
Mika Prunnila**[1]

[1] VTT Technical Research Centre of Finland, PO Box 1000, FI-02044 VTT, Espoo, Finland
[2] Low Temperature Laboratory, O V Lounasmaa Laboratory, Aalto University School of Science,
PO Box 15100, FI-00076 Aalto, Finland
[3] Department of Applied Physics, Aalto University School of Science, PO Box 11100, FI-00076, Aalto,
Espoo, Finland

E-mail: david.gunnarsson@vtt.fi

Abstract
We have measured the excited state lifetimes in Josephson junction phase and transmon
qubits, all of which were fabricated with the same scalable multi-layer process. We have
compared the lifetimes of phase qubits before and after removal of the isolating dielectric,
SiN_x, and find a fourfold improvement of the relaxation time after the removal. Together with
the results from the transmon qubit and measurements on coplanar waveguide resonators,
these measurements indicate that the lifetimes are limited by losses from the dielectric
constituents of the qubits. We have extracted the individual loss contributions from the
dielectrics in the tunnel junction barrier, AlO_x, the isolating dielectric, SiN_x, and the substrate,
Si/SiO_2, by weighting the total loss with the parts of the electric field over the different
dielectric materials. Our results agree well with and complement the findings from other
studies, demonstrating that superconducting qubits can be used as a reliable tool for
high-frequency characterization of dielectric materials. We conclude with a discussion of how
changes in design and material choice could improve qubit lifetimes by up to a factor of 4.

(Some figures may appear in colour only in the online journal)

1. Introduction

A great deal of research has recently been dedicated to scaling up quantum computers from a few qubit regime to networks of quantum bits. These efforts have concentrated both on creating more robust qubit designs and on better controlling the environmental non-idealities. Josephson junction (JJ) qubits, which include phase qubits [1, 2], flux qubits [3], transmon [4, 5], quantronium [6], and charge qubits [7, 8], are contenders in this effort of increasing the complexity of quantum electronics. In the first JJ qubit experiments, the coherence times were a few ns [6] and today, around one decade later, dozens of μs have been reported [9]. This impressive development comes from improvements in circuit design, with new ideas for devices [4, 6, 10, 11] and from thorough material research [12–15].

From the perspective of reaching a scalable solution for multiple JJ qubits, fabrication by multi-layer technology seems preferable. For these qubits, the isolating material between the layers and the large tunnel junction sizes increase the coupling to unwanted degrees of freedom. A lot of work has been done to investigate these decoherence mechanisms and to quantify the quality of materials [12–16]. One limitation for these qubits originates from dielectric losses due to two-level systems (TLS), acting as electric dipoles [12, 16, 17]. In the frequency regime of multi-layer JJ qubits, 1–10 GHz, electric losses in the dielectrics are dominated by dipole relaxations. The dissipation can be quantified and measured through the loss factor, $\tan \delta$, which can also be used to quantify the lifetimes of qubits that are limited by relaxation to TLS [12].

In this paper, we quantify the losses resulting from dielectric layers in two different qubit systems, a phase and a transmon qubit, made within the same multi-layer process. We have used their respective excited state lifetimes, combined with measurements of the photon lifetimes in coplanar waveguide (CPW) resonators, to extract the dielectric losses of the materials used at ultra-low temperature and with small probe powers. Unlike similar studies, ours has also correlated the reduction of dielectric materials through sample post-processing to greatly improve the qubit lifetime. It is worth noting that often the quality of devices goes down when more steps are added to a process. Measurements from two different qubit types and CPWs have been used to quantify the quality of a highly scalable production process [18].

2. Experimental details

Both Josephson junction phase qubits and transmon qubits [1, 2, 4, 5] were fabricated on thermally oxidized 625 μm thick, 50 Ω cm p-type Si substrates. The 300 nm thick thermal oxide was grown at 1000 °C by wet oxidation. Tunnel junctions of the qubits have AlO$_x$ tunnel barriers and sputter deposited Al top and bottom electrodes (see figures 1(a) and (b)). Tunnel junction area is defined by a through dielectric via process described and characterized in detail in [18]. We followed the process of [18] except that here we used 250 nm SiN$_x$ dielectric (deposited by plasma enhanced chemical vapour deposition at 180 °C). All patterns have been defined using UV lithography. The transmon Josephson junctions were configured in a SQUID geometry with a nominal junction area $A_j = 0.5$ μm^2 (see figures 2(a) and (b)), shunted with an interdigital capacitor (IDC), C_s^t, and embedded into a CPW resonator designed for $f_c \simeq 5$ GHz (for device parameters, see table 1). The charging energy is defined through $E_C = e^2/2C_\Sigma$, where C_Σ is the qubit total capacitance [4]. The phase qubits were made with the same technology, with the addition of a metallic bridge layer for galvanic contact between bottom and top Al layers. This adds two process steps, definition of vias in the SiN$_x$ and a bridge metallization of Al through lift-off (see figure 1(a)). The phase qubits were made with the Josephson junction in a RF-SQUID configuration, with a nominal junction area of 1.7 μm^2, and coupled to an asymmetric DC-SQUID for read-out [2] (see figures 2(c) and (d)). The Josephson junction was shunted with an IDC, C_s^{PQ}. Measurements were made for two different phase qubits, PQ-A and PQ-B. For sample PQ-A the SiN$_x$ is left, while for sample PQ-B a final etch step with CF$_4$ + O$_2$ plasma was applied for complete removal of the SiN$_x$ covering the IDC and surrounding the tunnel junction area. The removal gives rise to the change in total capacitance. The phase qubits are also coupled to $f_c = 6$ GHz CPW resonators, but they were far detuned and not considered in these studies. Even though we compare two JJ qubits from different regimes (phase and intermediate charge–flux qubits), their tunnel junction barriers have similar physical dimensions, and hence they can be regarded as similar from a material point of view and in the analysis of the dielectric losses.

Measurements have been made on five different devices—two CPWs, two PQs and one transmon—with
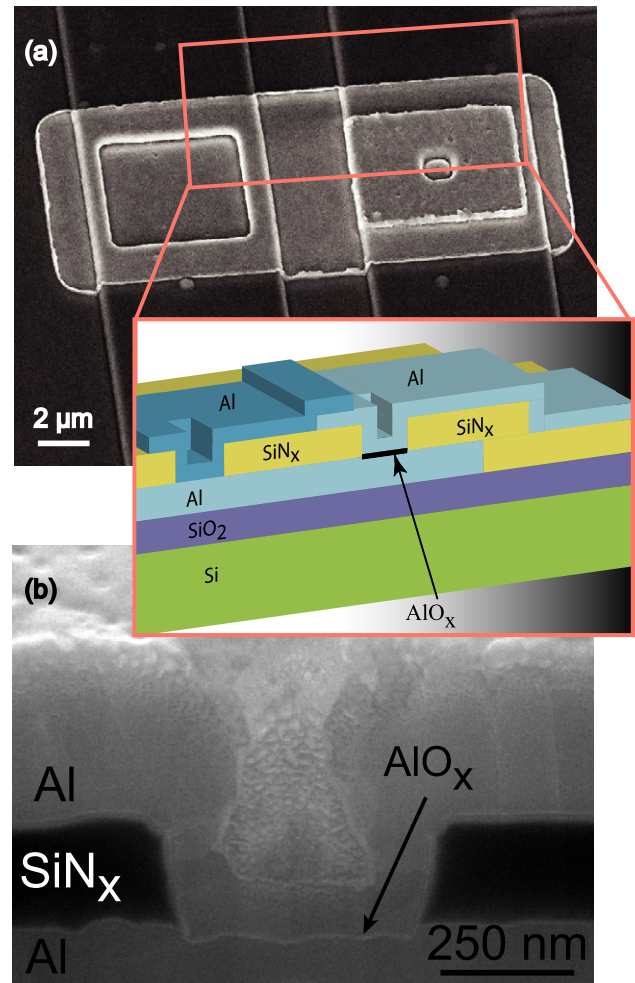

Figure 1. (a) SEM micrograph top view shows the tunnel junction (right) and the via (left). The inset illustrates the multi-layers and via in an illustrated cut view. (b) A SEM micrograph after a focused ion beam cut through the tunnel junction.

different parameters to get information about the losses. The measurements for the devices have been made at different frequencies in the range 3–10 GHz at the base temperature (~30 mK) of a dilution refrigerator. All measurements have been performed with low energy excitations with $V_{rms} < 1$ μV.

The CPW resonators were designed as 1.26 cm long transmission lines of 50 Ω characteristic impedance, terminated with $C_c = 5$ fF coupling capacitors at both ends. They were characterized by transmission measurements in order to extract the resonance peak linewidth that defines the loaded Q value, Q_L. The CPW resonators are under-coupled and the intrinsic Q value, Q_0, is determined by $Q_0 = Q_L/(1 + S_{21}(f_c))$ where $S_{21}(f_c)$ is the measured insertion loss [19].

For the qubits we have measured the excited state lifetime through the decay time after π-pulse Rabi excitations [6]. The transmon measurement was realized by a two-tone excitation technique, where both a measurement signal and the Rabi pulse were sent through the CPW resonator. The read-out of the transmon was done in the weak dispersive limit [20], with CPW coupling $g/2\pi \sim 40$ MHz and CPW
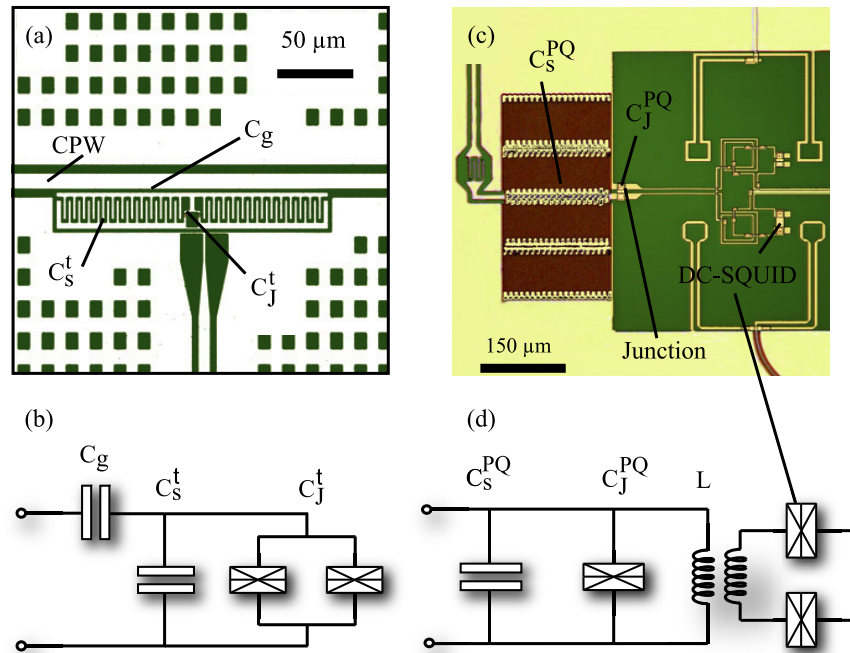
Figure 2. In (a) the optical microscope image of a transmon qubit, showing both the CPW resonator and the coupled JJ qubit. The schematic diagram for the transmon qubit is drawn in (b). In (c) and (d) the same illustrations are presented for the phase qubit layout and its schematics.

Table 1. Sample parameters. The parameters that are not applicable are marked with '×', and non-relevant ones with '—'. The tunnel junction areas A_j indicate the nominal values and the tunnel junction resistance R_j is measured from an on-chip test junction. The values of the Josephson coupling energy, E_J, are extracted from R_j through the Ambegaokar–Baratoff relation [23]. Total capacitances, C_Σ, are estimated from the circuit designs. C_Σ can also be estimated from frequency spectroscopy measurements, with the aid of estimates of E_J. The error bounds for C_Σ when using E_J for the calculation are hard to estimate compared to the geometrical capacitances, which we have used here.

	A_j (μm^2)	R_j (kΩ)	C_Σ (fF)	E_C/h(GHz)	E_J/h(GHz)	f_c(GHz)	f_{01}(GHz)	T_1(ns)	Q	$\tan\delta$
CPW A	×	×	—	×	×	5.09	×	×	15 593	6.2×10^{-5}
CPW B	×	×	—	×	×	5.02	×	×	16 225	6.4×10^{-5}
Transmon A	1.0	4.2	97	0.21	33	5.00	3.01	131	2 474	4.0×10^{-4}
PQ-A	1.7	0.14	697	0.027	1080	×	7.86	31	1 531	6.5×10^{-4}
PQ-B	1.7	0.16	581	0.033	870	×	10.3	130	8 413	1.2×10^{-4}

detuning $\Delta \sim 2$ GHz. For the phase qubit measurements, the Rabi excitation was applied with a flux bias line which is inductively coupled to the JJ loop (figures 2(c) and (d)). The read-out was done by applying a short read-out flux pulse to the JJ, which discriminates between the ground and excited state of the qubit. This long lived state was then measured with the inductively coupled DC-SQUID. The phase qubit energy level spectroscopy data in figure 3 were obtained by sweeping the frequency and the applied flux bias. The spectroscopy data illustrate the single-photon transitions between the qubit ground and excited state. A more thorough analysis of hybrid TLS–qubit systems, from spectroscopy and time-domain measurements, can be found in [21, 22].

3. Results and discussion

3.1. Relaxation times and quality factors

CPW resonators: For the two CPW resonators on which measurements were made we get a $Q_0 \sim 16\,000$, at resonance
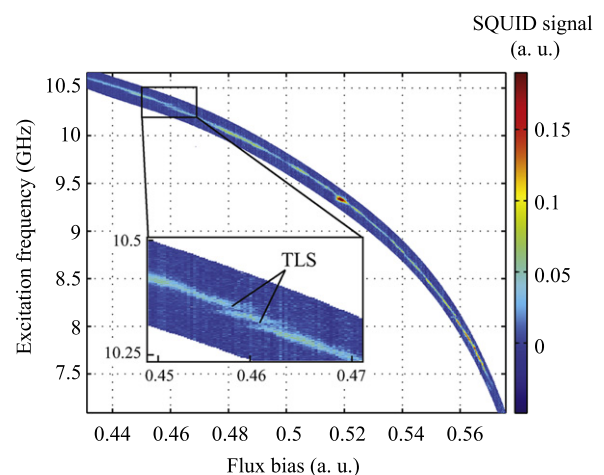

Figure 3. Spectroscopy of phase qubit PQ-A. In the enlargement, two avoided level crossings due to single-photon transitions between the qubit and TLS are indicated.
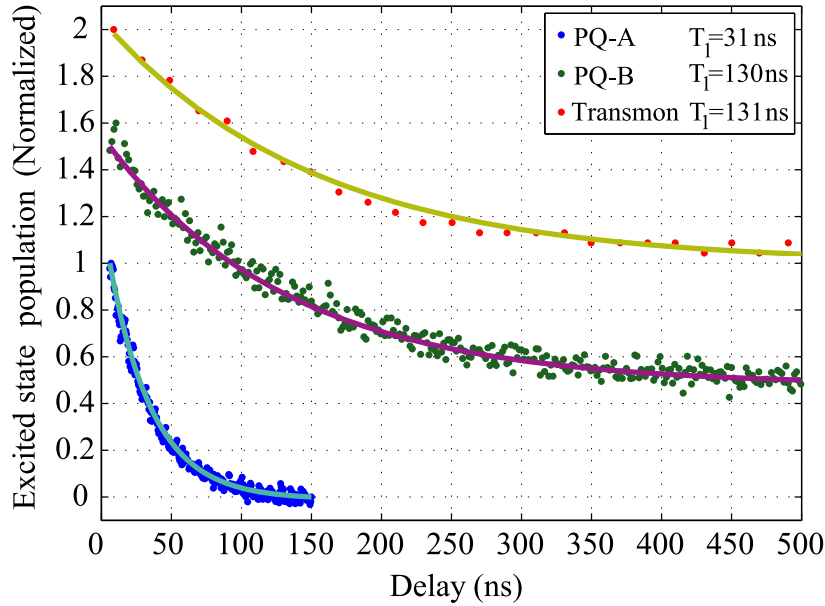
Figure 4. Excited state population as a function of delay time after a π-pulse for the three qubit samples. Solid lines denote the corresponding fits to exponential decay. The curves are shifted in the *y*-direction for clarity.

frequency $f_c \sim 5$ GHz (see table 1). The losses agree well with what has been obtained in earlier studies [13] for double-layered substrates with Si and 300 nm thermal SiO_2, where the resonators are assumed to be limited by the dielectric losses of the substrate.

Transmon: The excited state population as a function of delay time, after a π-pulse from the ground state, is shown in figure 4. The relaxation time, T_1, was measured to be $T_1 = 131$ ns at an energy level separation corresponding to $f_{01} = 3$ GHz. This is well below the expected T_1 for this design of qubit [4, 5], with regard to CPW resonator–qubit coupling and influence from control and back-action, which limits the T_1 to a few μs. We attribute the limiting factors to dielectric material losses, also in agreement with other multi-layer processing of transmon qubits [24]. Indeed, typical transmon qubits with long T_1 are fabricated on low-loss sapphire substrate, with ultra-small tunnel junctions and with no deposited dielectric layers [5].

Phase qubits: The decay time measurements for the two phase qubit samples, PQ-A and PQ-B, gave $T_1 = 31$ ns at $f_{01} = 7.9$ GHz and $T_1 = 130$ ns at $f_{01} = 10.3$ GHz, respectively (see figure 4). Here the large improvement for PQ-B is attributed to the removal of the deposited SiN_x.

3.2. Loss estimation

We use the model for the dielectric losses based on electrical dipole TLS residing in the dielectrics to evaluate our qubits [12, 17]. An example of this loss mechanism can be found in the enlargement of the spectroscopy data in figure 3, as the avoided level crossings from qubit–TLS interaction. It is valuable to get an upper estimate on how much the different dielectrics, AlO_x, SiN_x, and SiO_2/Si, contribute to the total loss of the qubits. Since the coupling is through electric field, the main loss is due to the electric field inside

a dielectric or, equivalently, electric energy stored on the capacitive elements of the devices. The dielectric losses for a capacitor can be expressed with a complex permittivity $\varepsilon = \varepsilon_1 - i\varepsilon_2$, where $\tan\delta = \varepsilon_2/\varepsilon_1$. The qubits can be modelled as parallel *LC*-resonators, where the nonlinear inductance and capacitance are defined through the Josephson junction and the geometrical surroundings. At resonance the electric energy of the resonator is $E_e = \frac{|V_{rms}|^2}{4}C_\Sigma$. In table 1, the relaxation times for our devices have been recalculated into equivalent tangent loss factors, through the relations $Q = 2\pi f_{01} T_1$ and $\tan\delta = 1/Q$ [12]. By weighting the contributions from the different dielectrics to the total loss, with their respective capacitance fraction of the total capacitance, we can extract the material loss factors [24]. The total loss can be written as

$$\tan\delta = \sum_i P_i \tan\delta_i,$$

where $P_i = C_i/C_\Sigma$ is the capacitance fraction for the *i*th included dielectric, C_i and $\tan\delta_i$ its respective capacitance and loss tangent, and C_Σ the total capacitance.

Our qubits contain both IDC and plate capacitor (tunnel junction) geometries (see figures 2(c) and (d)). To get the individual capacitances we have estimated them from well-known geometrical methods. For the IDCs we have used the method of conformal mapping to get the capacitance on multi-layer dielectric stacks [25, 26]. For the IDCs in particular, we have used this method to estimate how large a fraction of the electric energy is stored in the covering SiN_x layer and the substrate, respectively. The dielectric thicknesses are $t_{SiO_x} = 300$ nm and $t_{SiN_x} = 250$ nm and we have used dielectric constants $\varepsilon_{SiN_x} \simeq 7.5$, $\varepsilon_{SiO_2} \simeq 3.9$ and $\varepsilon_{Si} \simeq 11.9$. 19% of the energy of the IDC is stored in the SiN_x, 71% in the substrate SiO_x and Si stack and the remainder in the vacuum. SiN_x also plays a role in the transmon, and from a similar estimation the energy stored in the IDCs SiN_x is $\sim$7%.

Table 2. Capacitances and weight factors. The qubits consist of two main capacitors, the tunnel junction capacitance, C_j, and a shunt capacitance, C_s. The top part of the table shows the estimated capacitances for each device. The lower part shows the weights for the different dielectrics. The weight for SiN_x comes from the fraction of energy stored in the SiN_x surrounding the IDC shunts, C_s. For PQ-B, the SiN_x was removed by post-processing (see section 2).

Capacitance	Transmon	PQ-A	PQ-B	CPW A & B
Tunnel junction (fF)	$C_j = 60$	$C_j = 101$	$C_j = 101$	$\times$
Shunt IDC (fF)	$C_s = 26$	$C_s = 596$	$C_s = 480$	$\times$
Coupling (fF)	$C_g = 11$	$\times$	$\times$	$\times$
P_{AlO_x} (%)	61	14	17	0
P_{SiN_x} (%)	3	20	0	0
P_{sub} (%)	36	66	83	100

Table 3. Tangent loss parameters of different materials obtained from the fitting. The errors arise from the geometrical uncertainties in our capacitance estimates, and represent the worst case from propagating errors.

Material	$\tan \delta$
AlO_x	$4.8 \times 10^{-4} \pm 2.0 \times 10^{-4}$
SiN_x	$30 \times 10^{-4} \pm 5.0 \times 10^{-4}$
Substrate	$0.6 \times 10^{-4} \pm 0.3 \times 10^{-4}$

The capacitances for the tunnel junctions we have estimated with a value of 60 fF μm^{-2}, which is the value obtained from measurements on 0.5–2 μm^2 tunnel junctions made with the same process [18]. We have excluded capacitances that contribute <1% to C_Σ. The included capacitances and the material weights are presented in table 2. The CPW resonators are made in the last steps of processing, and we assume them to be limited by the losses from the substrate dielectrics.

The fitting procedure is a least square method for the linear system of equations having the form $\mathbf{Ax} = \mathbf{b}$, with $\mathbf{A}$ being the matrix of material weights; $\mathbf{b}$ is a vector with elements of the measured loss and $\mathbf{x}$ is the fitted vector of $\tan \delta$ for the dielectrics of our process:

$$
\overbrace{\begin{bmatrix} P_{AlO_x}^{CPWA} & P_{Sub}^{CPWA} & P_{SiN_x}^{CPWA} \\ P_{AlO_x}^{CPWB} & P_{Sub}^{CPWB} & P_{SiN_x}^{CPWB} \\ P_{AlO_x}^{PQA} & P_{Sub}^{PQA} & P_{SiN_x}^{PQA} \\ P_{AlO_x}^{PQB} & P_{Sub}^{PQB} & P_{SiN_x}^{PQB} \\ P_{AlO_x}^{t} & P_{Sub}^{t} & P_{SiN_x}^{t} \end{bmatrix}}^{\mathbf{A}} \overbrace{\begin{bmatrix} \tan \delta_{AlO_x} \\ \tan \delta_{Sub} \\ \tan \delta_{SiN_x} \end{bmatrix}}^{\mathbf{x}}
$$

$$
= \overbrace{\begin{bmatrix} \tan \delta_{CPWA} \\ \tan \delta_{CPWB} \\ \tan \delta_{PQA} \\ \tan \delta_{PQB} \\ \tan \delta_{t} \end{bmatrix}}^{\mathbf{b}}. \tag{1}
$$

We include all data from the qubits and the CPW resonators in the fit. In table 3, the solutions $\mathbf{x}$, $\tan \delta$ for the dielectrics are presented and we find that the losses are in good agreement with results from similar measurements from other groups [13, 14, 24].

This analysis is based on the estimated values of the capacitances with errors that can be quantified. The

uncertainty in the lateral dimensions of our process is <20%, which will introduce errors in the capacitance estimates for both the IDCs and tunnel junctions. For the tunnel junctions, additional uncertainty comes from using the measured junction capacitances from similar devices, which we estimate to be <40%. We have made an error analysis by allowing an input uncertainty of the capacitance values according to the dimension uncertainties from the process. In table 3, the resulting propagating errors of the fit are included. The uncertainties fall within reasonable limits and do not change the conclusions from our analysis. A comparison of how the different dielectrics contribute to the total loss can be found table 4. The sum of each device's loss contributions in table 4 agrees well with the measured losses (see table 1). It is important to point out that the results from the different samples have been measured at different frequencies (see table 1), but the distribution in the number of TLS and strengths of coupling to the qubits has been reported to be fairly uniform in this frequency range [12, 21].

The number and strength of avoided level crossings seen in the spectroscopic data (see figure 3) can be used to compare our results from relaxation time measurements [12]. We find a defect density $\sigma h \sim 2.4$ (GHz μm^2)$^{-1}$ and the maximum level splitting $S_{max}/h \sim 0.02$ GHz from samples PQ-A and PQ-B and this gives a lifetime, $T_1 \sim 185$ ns. Here we have used the relation $1/T_1 = (\pi/6)\sigma A S_{max}^2/\hbar$ derived in [12], which describes the lifetime in tunnel junctions from the strength and density of avoided level crossings. Translated into dielectric loss factors for the tunnel junctions in PQ-A and PQ-B the results are $\tan \delta_{AlO_x} = 1.1 \times 10^{-4}$ and $\tan \delta_{AlO_x} = 8.4 \times 10^{-5}$, respectively. Since the phase qubits seems to be limited by the additional losses to the SiN_x and substrate according to our analysis, we compare these values to the weighted loss tangents for AlO_x found in table 4. For PQ-B they are in very good agreement with the spectroscopic data, while there is a larger discrepancy for PQ-A. This is explained by the dominant loss to SiN_x for PQ-A compared to the almost equal loss to the substrate for PQ-B, which results in a greater error for the loss to AlO_x in PQ-A.

4. Summary and conclusions

By comparing the excited lifetimes and analysing the material losses, we were able to extract the contributions from different materials to the total loss of each device (see table 4). The result from the spectroscopic data also agrees well with our analysis, and hence strengthens its validity. For PQ-A it is

Table 4. The fitted losses attributed to the different dielectrics. The limiting losses for the different samples are indicated in bold letters. The losses for the two CPW resonators are the same, since all loss is assumed to be in the substrate.

	$P_{AlO_x}\tan\delta_{AlO_x}$	$P_{SiN_x}\tan\delta_{SiN_x}$	$P_{sub}\tan\delta_{sub}$	$\Sigma P_x\tan\delta_x$
PQ-A	6.9×10^{-5}	$\mathbf{5.5\times10^{-4}}$	3.4×10^{-5}	$6.5\times10^{-4}\pm1.3\times10^{-4}$
PQ-B	$\mathbf{8.4\times10^{-5}}$	0	$\mathbf{4.7\times10^{-5}}$	$1.3\times10^{-4}\pm4\times10^{-5}$
Transmon	$\mathbf{3.0\times10^{-4}}$	8×10^{-5}	2×10^{-5}	$4.0\times10^{-4}\pm1.4\times10^{-4}$
CPW A & B	0	0	$\mathbf{5.7\times10^{-5}}$	$5.7\times10^{-5}\pm3\times10^{-5}$

evident that the deposited SiN_x on top of the IDC contributes to its lower performance compared to sample PQ-B, where it has been removed. The lifetime of PQ-B is increased by more than a factor of 4, and is limited by the roughly equal losses coming from the AlO_x and the shunting IDC on the substrate. This indicates that post-processing steps, which potentially could be harmful to the tunnel junction quality, actually improve the qubit lifetime. The best phase qubits to date, based on multi-layer tunnel junction processing, have had the shunting IDC capacitor replaced by a plate capacitor with a low-loss dielectric made of a-Si:H. This gives lifetimes roughly three times better than those reported here [27]. An analysis similar to that done here indicates that these qubits are not limited by the dielectric losses, and it is speculated that losses are instead due to non-equilibrium quasiparticles [28]. From the data in table 4, it can be seen that the transmon qubit is clearly limited by the tunnel junction AlO_x quality, in its current design. Losses one order of magnitude lower were reported for micron-sized AlO_x tunnel junctions, with epitaxially grown Al_2O_3, where the transmon relaxation time was measured to be $T_1 = 0.76\ \mu s$ [24].

We have provided support for the assumption that material losses from dielectric layers limit the coherence of multi-layer JJ qubits. At the same time, these qubit coherence measurements can also be understood as a way to characterize the losses in materials at high frequency and low probe power. We have shown that this type of loss characterization works well for quantifying the quality of our highly scalable process, even with data from different qubit types. Previous work on various superconducting qubits has also indicated that among the sources of decoherence are the losses in the dielectric materials used for fabrication. However, different qubits were fabricated with different technologies and by different laboratories, and this diversity has precluded so far a clear comparison. In this paper we present for the first time a comparison between qubits of two different types fabricated with the same technology, thus allowing us to present a consistent picture of the effects of material losses in multi-layer JJ quantum bits. The information from our analysis should be helpful for improving future sample designs, where the limits of these materials can be approached. It should be possible for the phase qubits fabricated by means of this technology to reach values similar to those in [27], where the qubit performance is limited by other loss mechanisms [28]. The number of TLSs is proportional to the junction dimensions, and by reducing the tunnel junction size, the losses due to AlO_x can be reduced [12]. In combination with an increased IDC capacitance on optimized substrates, such as sapphire or low-loss Si [13], the phase qubit dielectric loss could be reduced by almost one order of magnitude, hence not being the limiting factor. Furthermore, for the transmon qubits, improvements of a factor of 3 could be obtained by using a low-loss substrate and reducing the tunnel junctions area to the limit of standard *i*-line projection lithography $\sim 0.5\ \mu m$. To approach quality similar to that for transmons fabricated with e-beam lithography with *in situ* double-angle evaporation, resulting in $T_1 > 2\ \mu s$, an improved process is needed. Such a process should have improved AlO_x quality, obtained for example with epitaxial AlO_x [15, 24], or utilize e-beam lithography for smaller tunnel junction definition.

Acknowledgments

References

[1] Martinis J M, Nam S, Aumentado J and Urbina C 2002 *Phys. Rev. Lett.* **89** 117901
[2] Cooper K B, Steffen M, McDermott R, Simmonds R W, Oh S, Hite D A, Pappas D P and Martinis J M 2004 *Phys. Rev. Lett.* **93** 180401
[3] Mooij J E, Orlando T P, Levitov L, Tian L, van der Wal C H and Lloyd S 1999 *Science* **285** 1036
[4] Koch J, Yu T M, Gambetta J, Houck A A, Schuster D I, Majer J, Blais A, Devoret M H, Girvin S M and Schoelkopf R J 2007 *Phys. Rev.* A **76** 042319
[5] Schreier J A *et al* 2008 *Phys. Rev.* B **77** 180502
[6] Vion D, Aassime A, Cottet A, Joyez P, Pothier H, Urbina C, Esteve D and Devoret M H 2002 *Science* **296** 886
[7] Nakamura Y, Pashkin Y A and Tsai J S 1999 *Nature* **398** 786
[8] Duty T, Gunnarsson D, Bladh K and Delsing P 2004 *Phys. Rev.* B **69** 140503
[9] Paik H *et al* 2011 *Phys. Rev. Lett.* **107** 240501
[10] Sillanpää M A, Lehtinen T, Paila A, Makhlin Yu, Roschier L and Hakonen P J 2005 *Phys. Rev. Lett.* **95** 206806
[11] Duty T, Johansson G, Bladh K, Gunnarsson D, Wilson C and Delsing P 2005 *Phys. Rev. Lett.* **95** 206807
[12] Martinis J M *et al* 2005 *Phys. Rev. Lett.* **95** 210503
[13] O'Connell A D *et al* 2008 *Appl. Phys. Lett.* **92** 112903
[14] Kline J S, Wang H, Oh S, Martinis J M and Pappas D P 2009 *Supercond. Sci. Technol.* **22** 015004
[15] Oh S, Cicak K, Kline J S, Sillanpää M A, Osborn K D, Whittaker J D, Simmonds R W and Pappas D P 2006 *Phys. Rev.* B **74** 100502R

[16] Cole J H, Müller C, Bushev P, Grabovskij G J, Lisenfeld J, Lukashenko A, Ustinov A V and Shnirman A 2010 *Appl. Phys. Lett.* **97** 252501

[17] Martin I, Bulaevskii L and Shnirman A 2005 *Phys. Rev. Lett.* **95** 127002

[18] Prunnila M, Meschke M, Gunnarsson D, Enouz-Vedrenne S, Kivioja J M and Pekola J P 2010 *J. Vac. Sci. Technol.* **28** 1026–9

[19] Pozar D M 1990 *Microwave Engineering* 3rd edn (New York: Wiley)

[20] Blais A, Huang R-S, Wallraff A, Girvin S M and Schoelkopf R J 2004 *Phys. Rev.* A **69** 062320

[21] Shalibo Y, Rofe Y, Shwa D, Zeides F, Neeley M, Martinis J M and Katz N 2010 *Phys. Rev. Lett.* **105** 177001

[22] Bushev P, Müller C, Lisenfeld J, Cole J H, Lukashenko A, Shnirman A and Ustinov A V 2010 *Phys. Rev.* B **82** 134530

[23] Ambegaokar V and Baratoff A 1963 *Phys. Rev. Lett.* **10** 486

[24] Weides M P *et al* 2011 *Appl. Phys. Lett.* **99** 262502

[25] Igreja R and Dias C J 2004 *Sensors Actuators* A **112** 291–301

[26] Igreja R and Dias C J 2011 *Sensors Actuators* A **172** 392–9

[27] Weides M *et al* 2011 *Supercond. Sci. Technol.* **24** 055005

[28] Martinis J M, Ansmann M and Aumentado J 2009 *Phys. Rev. Lett.* **103** 097002